Solid-solid Polymorphic Transition of 2,4,6,8,10,12-Hexanitro-2,4,6,8,10,12-hexaazaisowurtzitane (CL-20) at High Temperature by Metadynamics Simulations

Chaoyu Wang,[†,‡] Yuchuan Shi,[‡] Chaoyang Zhang,*[‡] Bo You,[†] and Xianggui Xue*[‡]

[†] College of Smart Materials and Future Energy, Fudan University, Shanghai 200433, China.

[‡] Institute of Chemical Materials, China Academy of Engineering Physics (CAEP), P.O. Box 919-311, Mianyang, Sichuan 621999, China.

Supplementary Information (SI)

Table of Contents

S1. Assessment of Force Field Accuracy for Polymorphs and Conformations.

First, the fundamental crystallographic parameters of different CL-20 polymorphs, including space group, unit cell dimensions, and density (A. T. Nielsen et al., *Tetrahedron*, **1998**, 54, 11793–11812), are summarized in Table S1.

Table S1. Crystallographic parameters of various CL-20 polymorphs, including ε-, β- and γ-CL-20.

	a (Å)	b (Å)	c (Å)	β (°)	Density (g/cm^3)	Space group
ε-CL-20	8.841	12.562	13.358	106.82	2.044	P21/C
β-CL-20	9.676	13.006	11.649	90.00	1.985	PCA21
γ-CL-20	13.231	8.170	14.876	109.17	1.916	P21/C

To validate the accuracy of the employed force field in describing the polymorphic structures and molecular conformations of CL-20, we compared the simulation results with experimental data.

Table S2. Comparison of simulated lattice parameters and densities of three CL-20 polymorphs using the refined force field with Experimental ones.

	ε-CL-20			β-CL-20			γ-CL-20		
	Exp	FF	Errors	Exp	FF	Errors	Exp	FF	Errors
a (Å)	141.453	139.406	-1.45%	77.408	80.536	4.04%	105.848	105.857	0.01%
b (Å)	75.373	73.806	-2.08%	78.036	73.936	-5.25%	65.360	62.870	-3.81%
c (Å)	26.715	27.222	1.90%	46.596	48.084	3.19%	44.628	45.400	1.73%
β (°)	106.82	106.25	-0.53%	90.00	90.00	-	109.17	108.83	-0.31%
Density (g/cm^3)	2.044	2.077	1.61%	1.985	1.95	-1.66%	1.916	1.96	2.08%

As Table S2 shown, it presents the calculated densities and lattice parameters (a, b, c, β) for various CL-20 polymorphs (ε-CL-20, β-CL-20, γ-CL-20), along with their relative deviations from experimental values. The simulation results show excellent agreement with experimental values, with a maximum deviation in density of only 2.08%, demonstrating that the employed force field accurately captures the crystal structures of CL-20.

In Table S3, except for the φ_3 in ε-CL-20, which shows a relatively large deviation of approximately 30°, all other key intramolecular angles exhibit deviations within 10° when compared to experimental data. Notably, despite the deviation observed for φ_3, its impact on distinguishing

molecular conformations and on the accuracy of phase transition simulations is minimal, as this angle plays a limited role in such processes. These findings further confirm the reliability of the employed force field in accurately representing both the molecular geometry and crystal structure of CL-20 polymorphs, supporting its suitability for subsequent phase transition studies.

Table S3. Comparison of the three angles (φ_1, φ_2, and φ_3) obtained from MD simulations with experimental measurements.

Rotation angles		Exp (degree,300K)	MD (degree,300K)
ε-CL-20	φ_1	95.16	96.31
	φ_2	145.68	145.06
	φ_3	50.02	82.66
β-CL-20	φ_1	38.57	30.66
	φ_2	82.67	78.85
	φ_3	28.66	22.32
γ-CL-20	φ_1	22.99	24.71
	φ_2	143.43	147.09
	φ_3	15.06	13.21

S2. Effect of System Size on Biasing Factor and Gaussian Height Settings.

In MetaD simulations, the choice of bias factor and Gaussian height plays a critical role in determining sampling efficiency and the convergence of the free energy surface. To identify a suitable set of MetaD parameters, we tested multiple parameter combinations and systematically evaluated their sampling efficiency and convergence behavior.

Initially, a bias factor of 100 and a Gaussian height of 50 k_BT were employed to perform a well-tempered metadynamics (WT-MetaD) simulation. As shown in Fig S1(a), neither the system volume nor the three key dihedral angles (φ_1, φ_2, φ_3) exhibited significant changes, indicating that under this parameter setting, the phase transition could not be driven even with extended simulation time and continued application of bias. This suggests insufficient sampling efficiency. We then increased the bias factor to 800 while keeping the Gaussian height at 50 k_BT. The results, shown in Fig S1(b), indicate that the system underwent a crystal phase transition within approximately 5000 Metadsteps (number of deposited Gaussians bias), and all three CVs (φ_1, φ_2, φ_3) were sampled accordingly. However, after 50000 Metadsteps, the fluctuations in CV sampling were significantly reduced, and transitions between different crystal phases became infrequent, suggesting that the MetaD simulation had not yet converged.

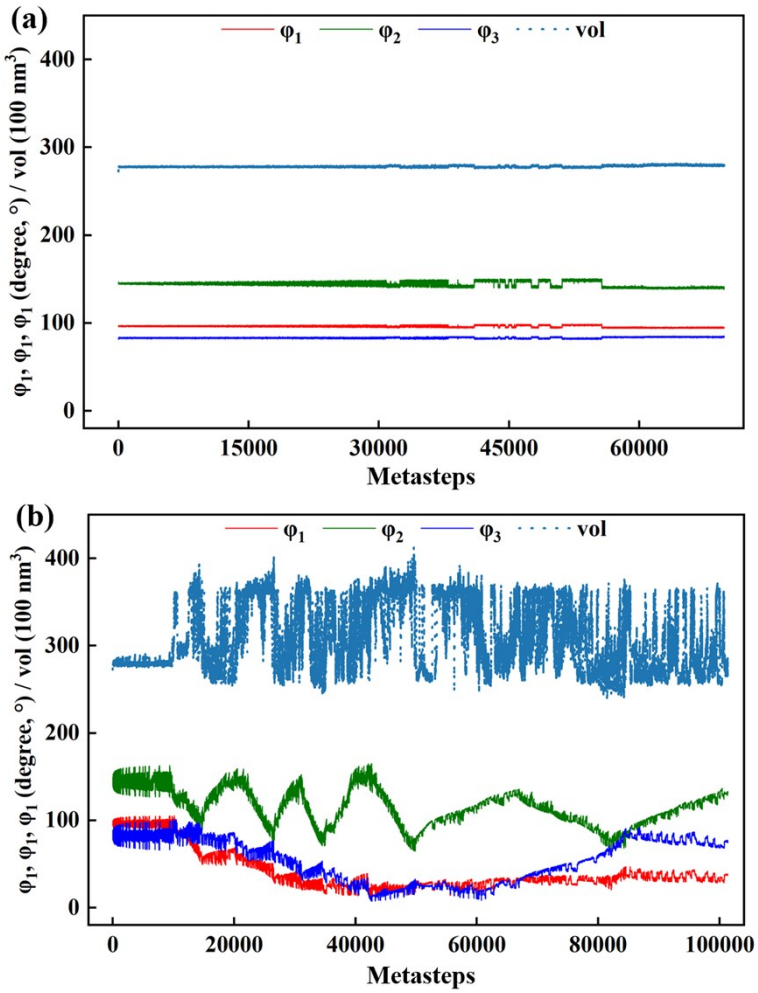

Figure S1. Time evolution of collective variables (CVs) during the CL-20 phase transition simulation as a function of bias deposition: (a) bias factor γ =100 and Gaussian height h = 50 k_BT; (b) bias factor γ =100 and Gaussian height h = 50 k_BT. The red, green, and blue curves represent the average values of the dihedral angles φ_1, φ_2, and φ_3 over 768 molecules, while the cyan curve shows the variation in system volume.

After extensive parameter testing, we determined that a Gaussian height of 30 k_BT and a bias factor of 12,000 enabled good convergence and sampling performance. Time evolution of the CVs is show in Fig S2.

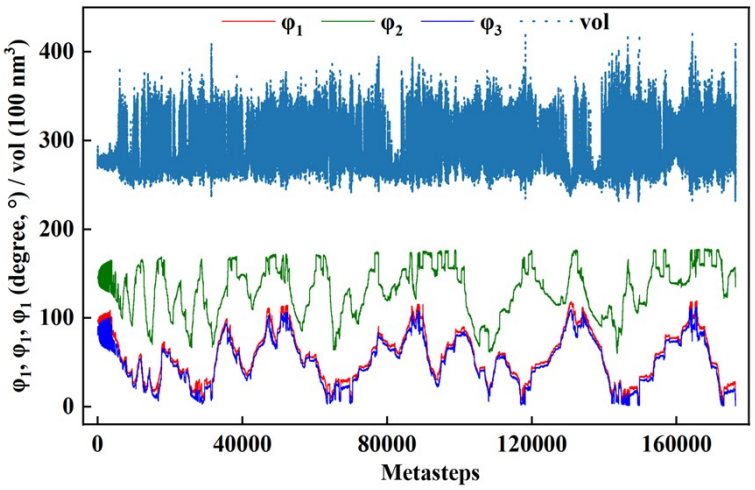

Figure S2. Time evolution (metasteps, number of Gaussian bias depositions) of the collective variables (CVs), with red, green, blue, and cyan curves representing φ_1, φ_2, φ_3 and volume, respectively.

However, the values of these parameters are significantly higher than the range suggested in the usual community standard. We believe that the choice of these two parameters is closely related to the size of the simulation system: the larger the system and the more molecules it contains, the higher the total free energy barrier associated with the phase transition. Therefore, we conducted an in-depth analysis of the relationship between parameter selection and system size, and established a theoretical quantitative relationship between the bias factor and Gaussian height with the total number of molecules in the system.

In the WT-MetaD framework, the height of the Gaussian bias potential is adaptively scaled at each step, with the degree of decay governed by a factor that depends on the accumulated bias energy. The expression for this decay factor is given by:

$$V(s,t_n) = \sum_{i=1}^{n-1} h e^{-V(s(q(t_i),\ t_i)/\Delta T} \exp\left(-\sum_{j=1}^{d} \frac{\left(s_j(q) - s_j(q(t_i))\right)^2}{2\sigma_i^2}\right) \tag{1}$$

Here, h is the Gaussian height, ΔT is the temperature parameter, d is the dimensionality of the CV space, and $V(s,t_n)$ is the cumulative bias at time t_n. For the CL-20 system in our study with N molecules, the bias potential becomes:

$$V_N(s,t_n) = \sum_{i=1}^{n-1} h_N e^{-V_N(s(q(t_i),\ t_i)/\Delta T_N} \exp\left(-\frac{\left(s(q) - s(q(t_i))\right)^2}{2\sigma_i^2}\right) \tag{2}$$

Similarly, for a system with M molecules, the bias potential is:

$$V_M(s,t_n) = \sum_{i=1}^{n-1} h_M e^{-V_M(s(q(t_i),\ t_i)/\Delta T_M} \exp\left(-\frac{\left(s(q) - s(q(t_i))\right)^2}{2\sigma_i^2}\right) \tag{3}$$

Assuming that both systems have converged and that each molecule experiences the same average bias, we obtain:

$$\frac{1}{N} V_N(s,t_n) \approx \frac{1}{M} V_M(s,t_n) \tag{4}$$

Similarly,

$$\frac{1}{N} V_N(s(q(t_i),t_i) \approx \frac{1}{M} V_M(s(q(t_i),t_i) \tag{5}$$

Substituting Equations (2), (3), and (5) into (4), and simplifying common terms, yields:

$$\frac{1}{N} h_N e^{-V_N(s(q(t_i),\ t_i)/\Delta T_N} \approx \frac{1}{M} h_M e^{-MV_N(s(q(t_i),\ t_i)/N\Delta T_M} \tag{6}$$

From this, we obtain the following approximate scaling relations:

$$h_N \approx \frac{N}{M} h_M, \quad \Delta T_N \approx \frac{N}{M} \Delta T_M \tag{7}$$

Accordingly, the bias factor scales as:

$$\gamma_N \approx \frac{N}{M} \gamma_M \tag{8}$$

In other words, both the Gaussian height and bias factor should scale approximately linearly with the number of molecules in the system. In our simulations, the system contains 768 CL-20 molecules, with a bias factor of 12,000 and a Gaussian height of 30 k_BT. If the system were scaled down to the smallest unit cell containing only 4 molecules, the corresponding parameters would be approximately 68 for the bias factor and 0.16 k_BT for the Gaussian height—both well within the reasonable range.

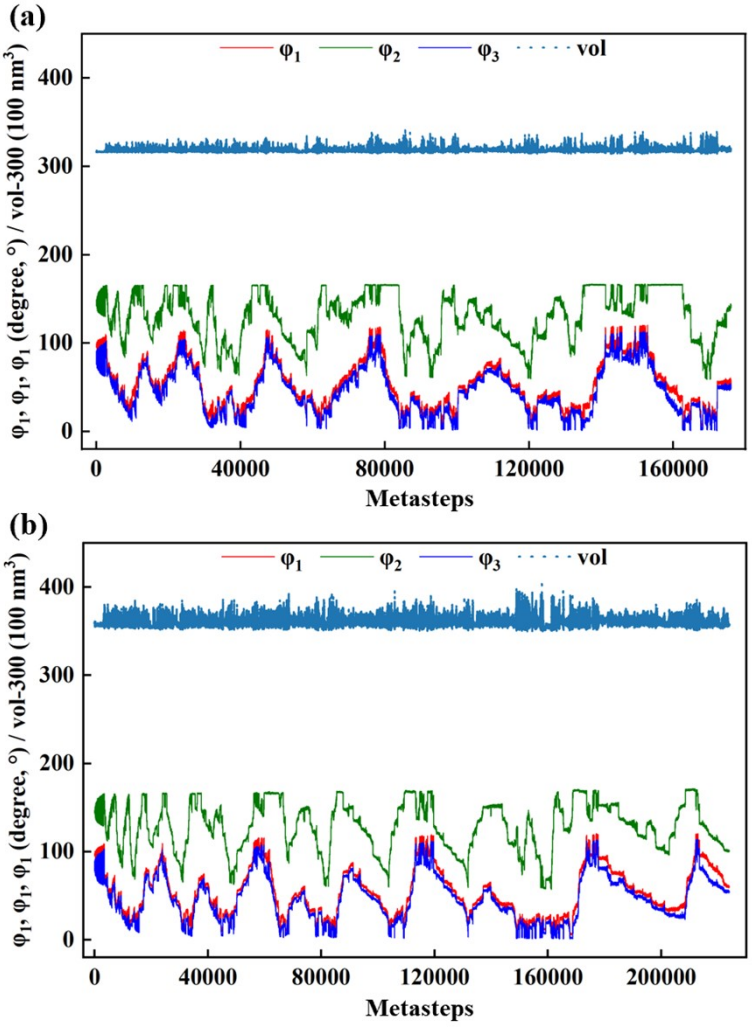

Figure S3. Time evolution of collective variables (CVs) during the CL-20 phase transition simulation as a function of bias deposition: (a) bias factor γ =750 and Gaussian height h = 2 k_BT; (b) bias factor γ =2250 and Gaussian height h = 6 k_BT. The red, green, and blue curves represent the average values of the dihedral angles φ_1, φ_2, and φ_3 over (a) 48 or (b) 144 molecules, while the cyan curve shows the variation in system volume.

To further validate these conclusions, we constructed two additional CL-20 supercells of

different sizes: 3×2×2 and 4×3×3, with corresponding lattice parameters a = 26.522 Å, b = 25.124 Å, c = 26.715 Å and a = 35.363 Å, b = 37.687 Å, c = 40.073 Å, containing 48 and 144 CL-20 molecules, respectively. According to our derived formulation, we assigned two sets of Gaussian heights and bias factors: 2 k_BT and 750; 6 k_BT and 2250, respectively. The CV evolution during simulations is shown in Fig S3. For both systems, the CVs exhibit multiple forward and backward fluctuations between different states, indicating sufficient sampling of the energy surface and good FES convergence. These results confirm the rationality and effectiveness of the selected Gaussian height and bias factor parameters and further validate the accuracy of our theoretical derivations.

S3. Order parameters (OPs) establishment for ε-, β- and γ-CL-20.

To distinguish the polymorphic characteristics of molecules, packing patterns is generally more general than molecular conformations. Therefore, in this study, we characterize CL-20 molecules in different polymorphs by establishing OPs, including molecular distance distributions, relative bond angle distributions, and relative orientation angle distributions, as shown in Fig S4.

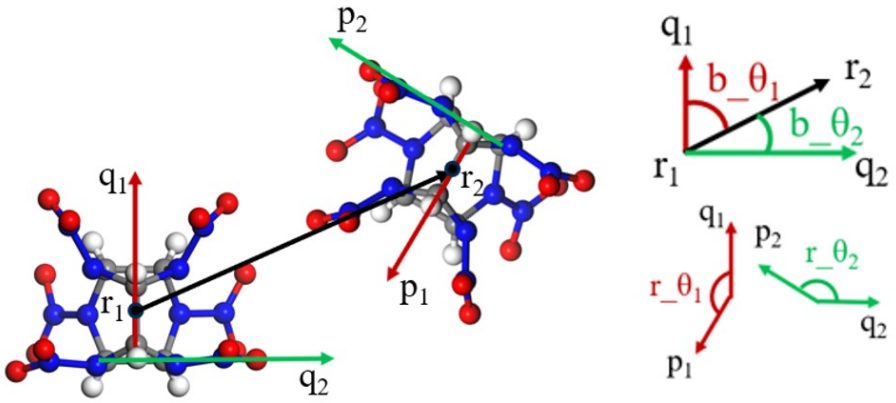

Figure S4. Schematic of the order parameter construction for CL-20.

Distance：
$$f_{\alpha}^{d}=\frac{1}{\sqrt{2\pi}\sigma_{d\alpha}^{2}}\exp\left[\frac{-(d-d_{\alpha})^{2}}{2\sigma_{d\alpha}^{2}}\right] \quad (1)$$

In the OPs expression of distance, d represents the distance between the molecule q of interest and any molecule p within the cutoff distance r. d_{α} denotes the value of the peak position, and $\sigma_{d\alpha}^{2}$ represents the corresponding variance. Generally, the number of peak positions is determined by the cutoff distance r, while the positions of the peaks are determined by the crystal structure.

Relative bond angle：
$$f_{\alpha}^{b\_\theta_i}=\frac{1}{\sqrt{2\pi}\sigma_{b\alpha i}^{2}}\exp\left[\frac{-\left(b\_\theta_i-b\_\theta_{\alpha_i}\right)^{2}}{2\sigma_{b\alpha i}^{2}}\right] \quad (2)$$

In the relative bond angle, the concept of bonds from atomic crystals is adopted. In its expression, b_θ_i represents the angle formed by the vectors from the center of mass of molecule q and molecule p on the local coordinate axis of molecule q, reflecting the spatial relative position of the two

molecules. $b\_\theta_{\alpha_i}$ and $\sigma_{b\alpha i}^{2}$ denote the peak value and variance, respectively.

Relative orientation angle：

$$f_{\alpha}^{r\_\theta_i} = \frac{1}{\sqrt{2\pi}\sigma_{r\alpha i}^{2}} \exp\left[\frac{-\left(r\_\theta_i - r\_\theta_{\alpha_i}\right)^2}{2\sigma_{r\alpha i}^{2}}\right] \tag{3}$$

(a) The distribution of distances within the cutoff radius.

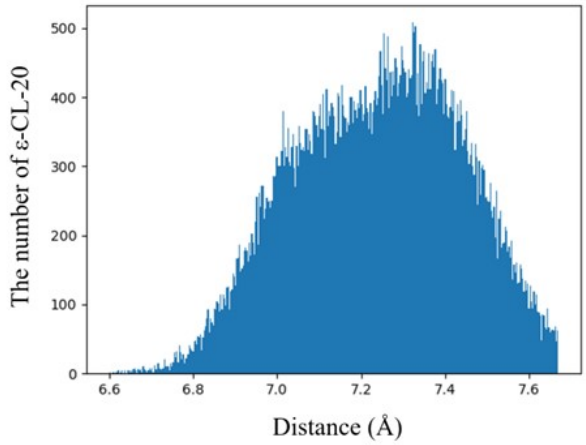

(b1) The distribution of relative bond angle formed by q_1-axis and p_1-axis.

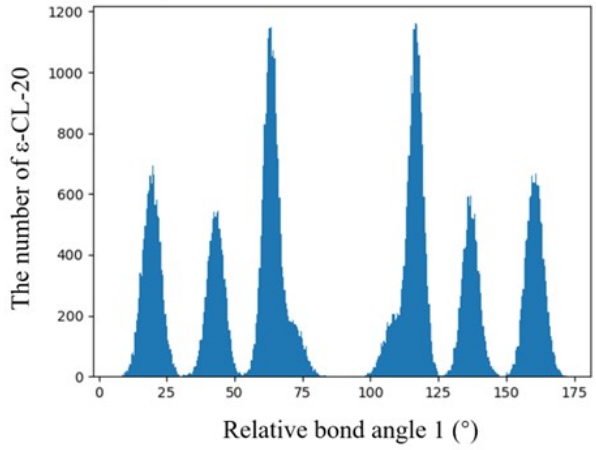

(b2) The distribution of relative bond angle formed by q_2-axis and p_2-axis.

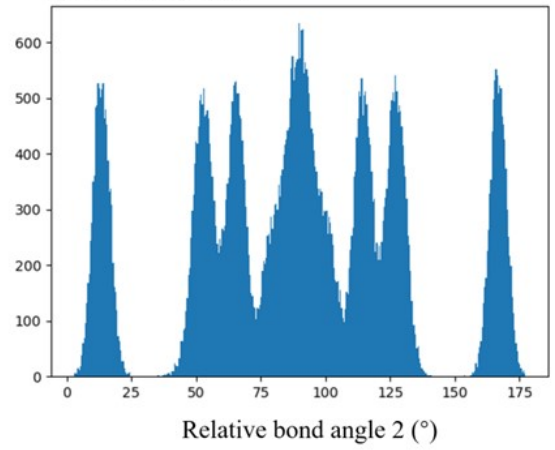

(c1) The distribution of relative orientation angle formed with the q_1-axis.

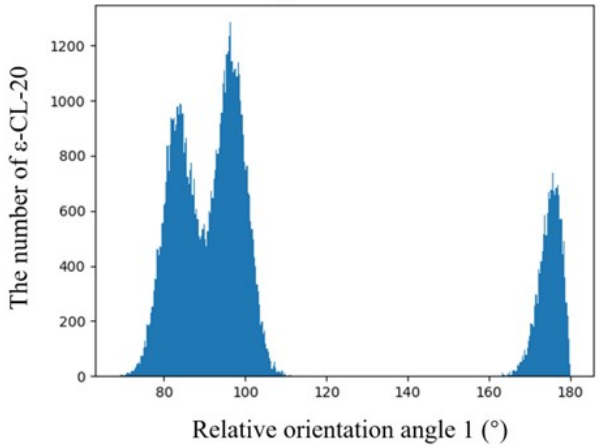

(c2) The distribution of relative orientation angle formed with the q_2-axis.

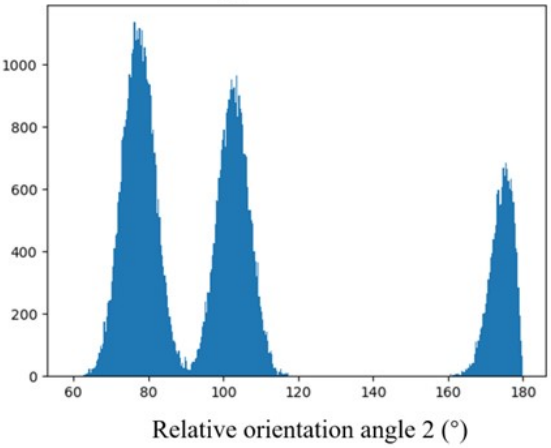

Figure S5. Histograms of molecular distances, relative bond angles, and relative orientation angles for ε-CL-20.

In the OPs expression of relative orientation angle, r_θ_i represents the angle between the corresponding axes in the local coordinate systems of molecules q and p, reflecting the relative orientation of the two molecules. $r\_\theta_{\alpha_i}$ and $\sigma_{r\alpha i}^2$ denote the peak value and variance, respectively.

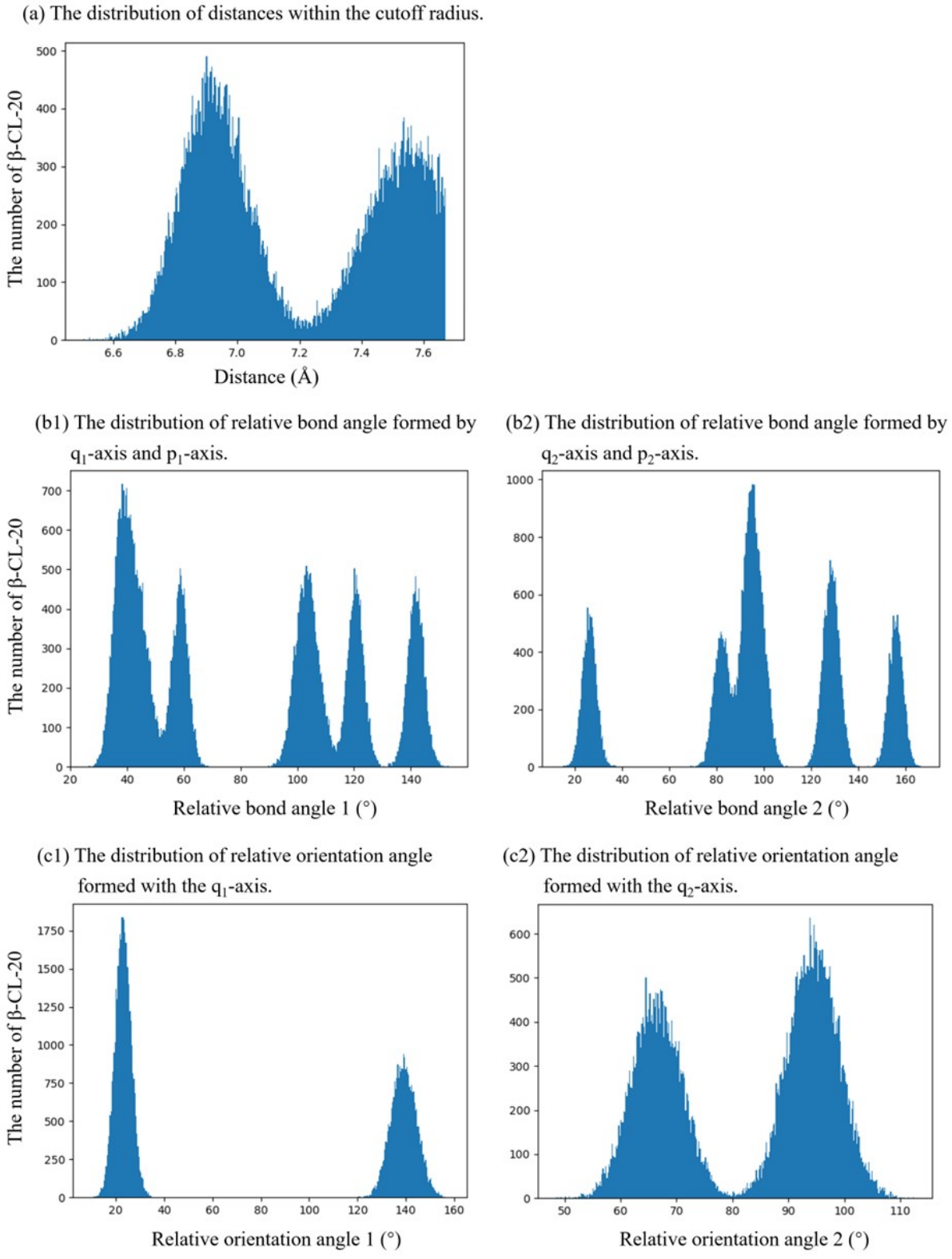

Figure S6. Histograms of molecular distances, relative bond angles, and relative orientation angles for β-CL-20.

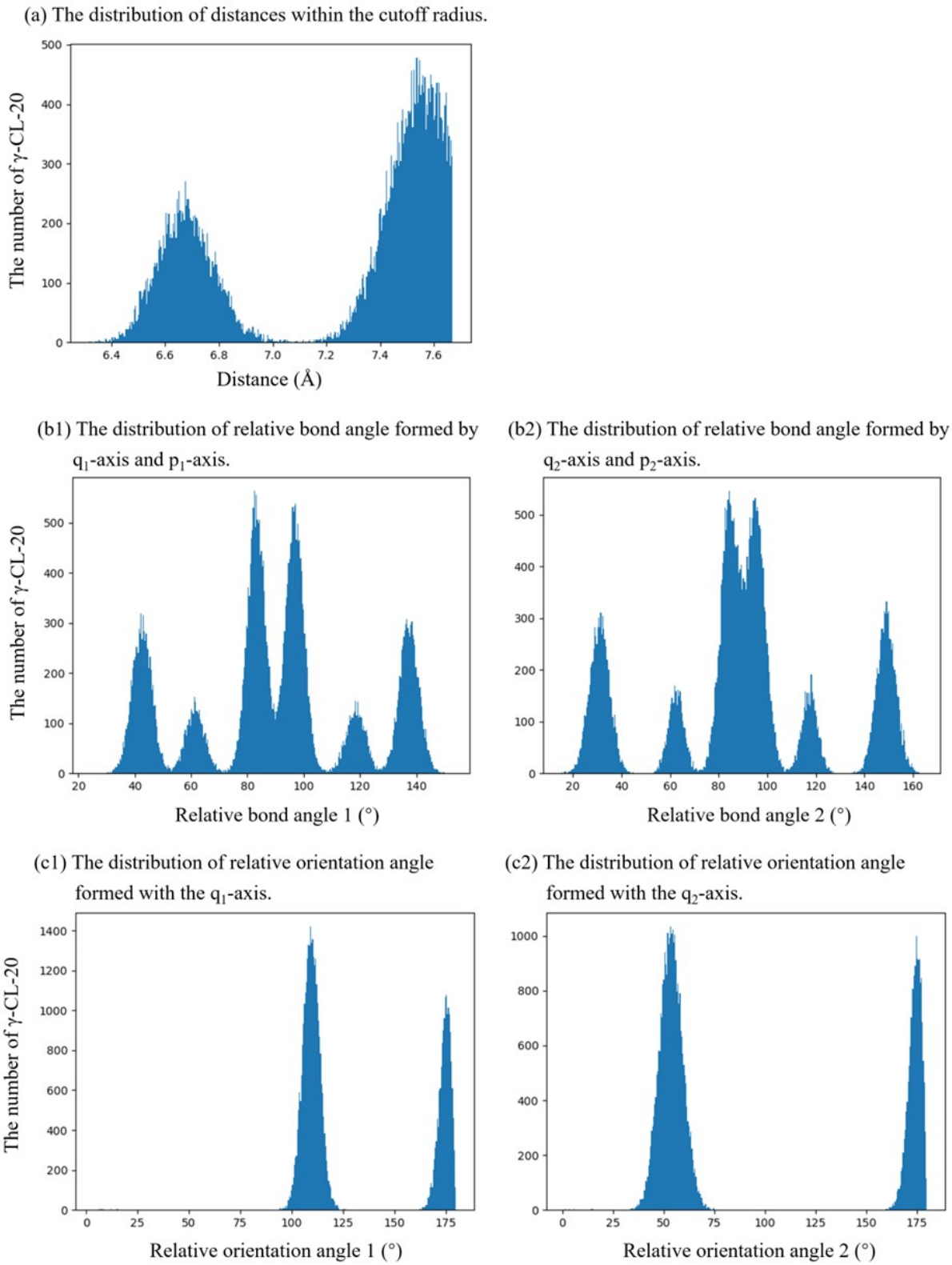

Figure S7. Histograms of molecular distances, relative bond angles, and relative orientation angles for γ-CL-20.

In this study, all OPs are represented using Gaussian distributions. To determine the mean and standard deviation of all OPs expression, statistical sampling was conducted through NPT molecular

dynamics (MD) simulations. The simulations were performed on supercell systems containing 768 molecules of ε-, β-, and γ-CL-20, and each simulation lasted for 500 ps. Trajectory files from the interval of 200 to 300 ps were sampled every 1 ps, resulting in 101 frames of coordinates. Subsequently, the OPs for each molecule in each frame were analyzed, with a cutoff radius set to 7.65 Å. Within this cutoff radius, distributions of molecular distances, relative bond angles, and relative orientation angles were statistically analyzed. The results are shown in Fig S5 to S7.

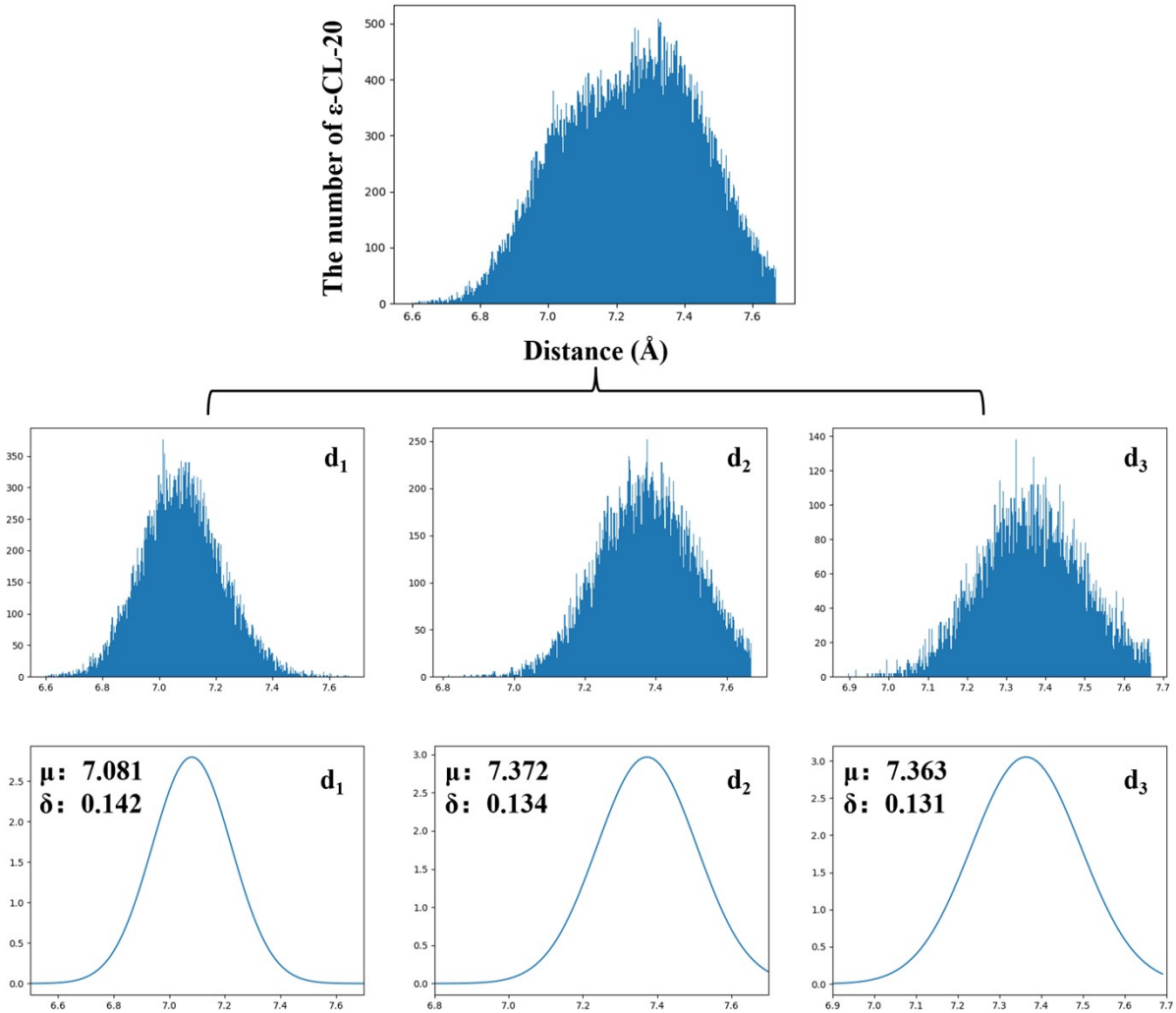

Figure S8. Schematic diagram of the Gaussian fitting and decomposition of the distance distribution for ε-CL-20.

Thereby, we decoupled and subsequently fitted them to derive the corresponding expressions. As shown in Fig S8, the distance distribution of ε-CL-20 within the cutoff radius can be decomposed into three individual Gaussian distributions. The mean and standard deviation of each distribution were calculated to obtain the parameters μ and σ for the Gaussian expressions. The resulting three

distribution equations are denoted as $g(d_1)$, $g(d_2)$, and $g(d_3)$.

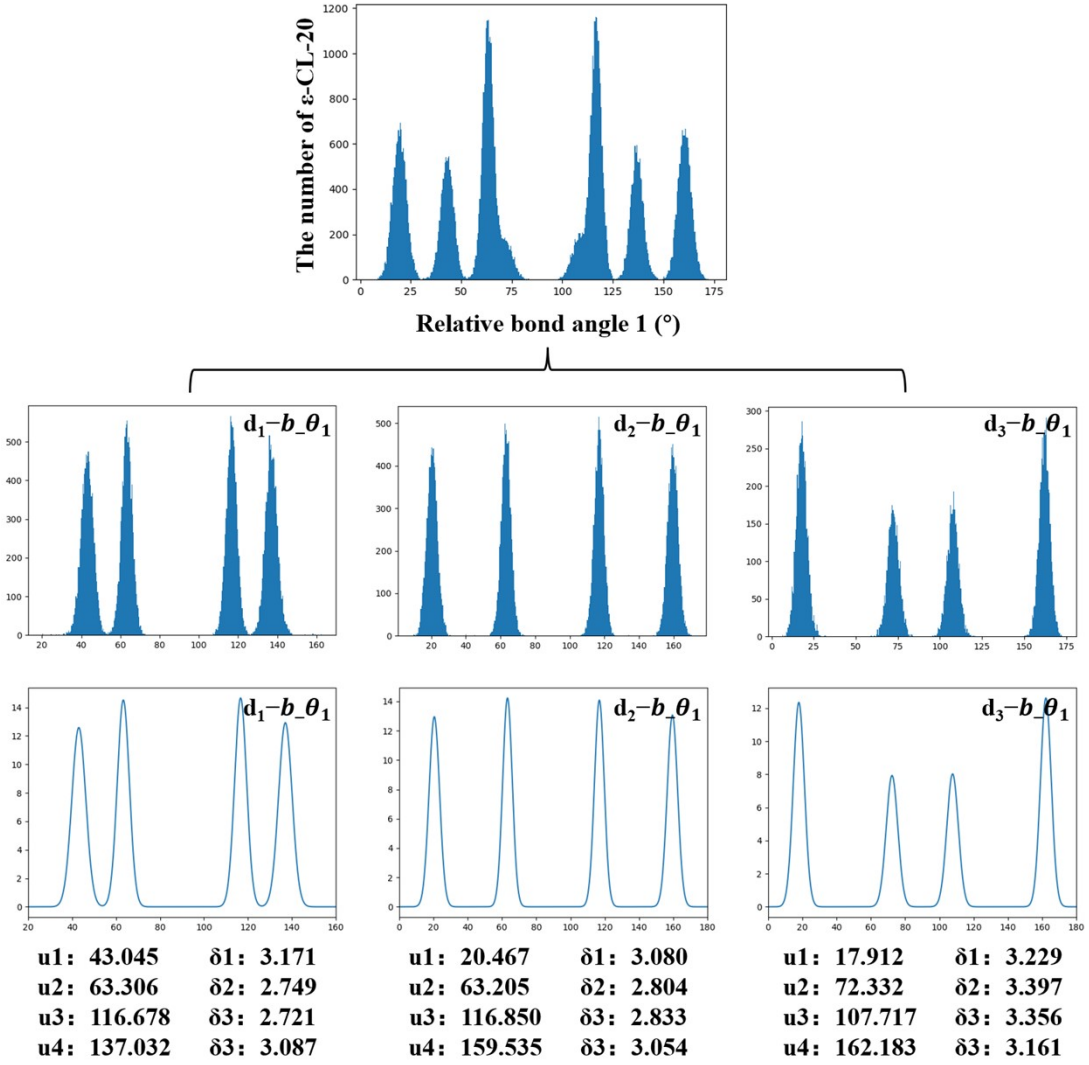

Figure S9. Schematic diagram of the Gaussian decomposition fitting for the relative bond angle 1 distribution in ε-CL-20.

Based on this, the corresponding Gaussian expressions for the relative bond angles and relative orientational angles were derived, with the specific decomposition illustrated in Fig S9 to S12. The relative bond angle distributions corresponding to the three distance distributions are very complex, with each relative bond angle distribution obtained by summing multiple Gaussian distributions. The expression is as follows:

$$g(d_j\text{–}b\_\theta_k) = \sum_{i=1}^{n} g(d_j\text{–}b\_\theta_k, \mu_i, \sigma_i)\ n = 3\ or\ 4;\ j = 1,2,3;\ k = 1,2 \quad (4)$$

In the Eq. 4, n represents the number of Gaussian functions included in each relative bond angle distribution, with all distributions containing four functions except for $d_2\text{–}b\_\theta_2$, which contains

three. The index j denotes the type of corresponding distance distribution, the index k represents the relative bond angles, where each distance distribution corresponds to two of them. Similarly, the relative orientational angle can be represented as $g(d_j\text{–}r\_\theta_k)$, with each one containing only one Gaussian function. The final expression for the OPs of ε-CL-20 is:

$$g(\varepsilon\text{–}CL\text{–}20) = \sum_{j=1}^{3}\left[g(d_j) \times \prod_{k=1}^{2} g(d_j\text{–}b\_\theta_k) \times \prod_{k=1}^{2} g(d_j\text{–}r\_\theta_k)\right] \quad (5)$$

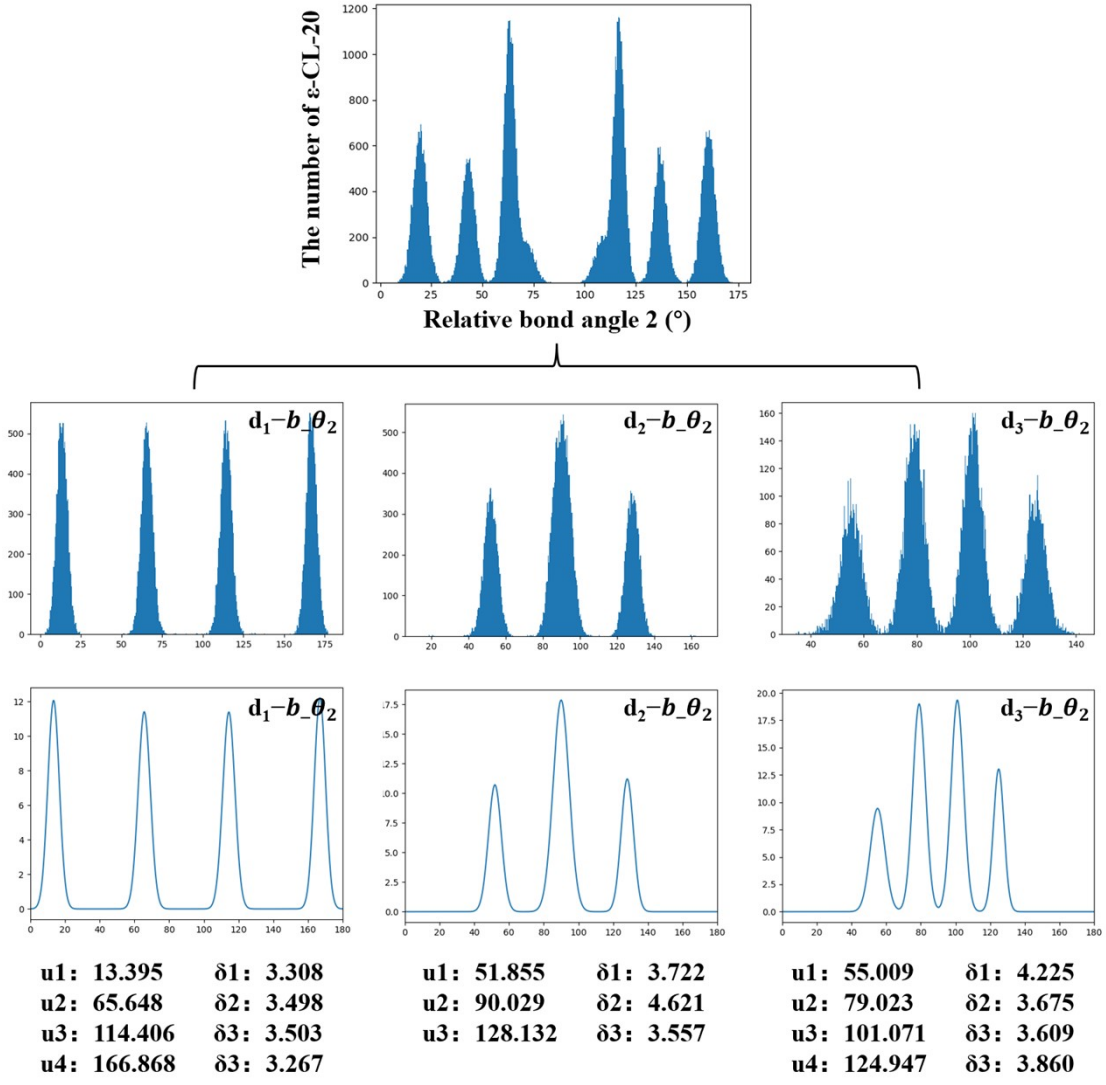

Figure S10. Schematic diagram of the Gaussian decomposition fitting for the relative bond angle 2 distribution in ε-CL-20.

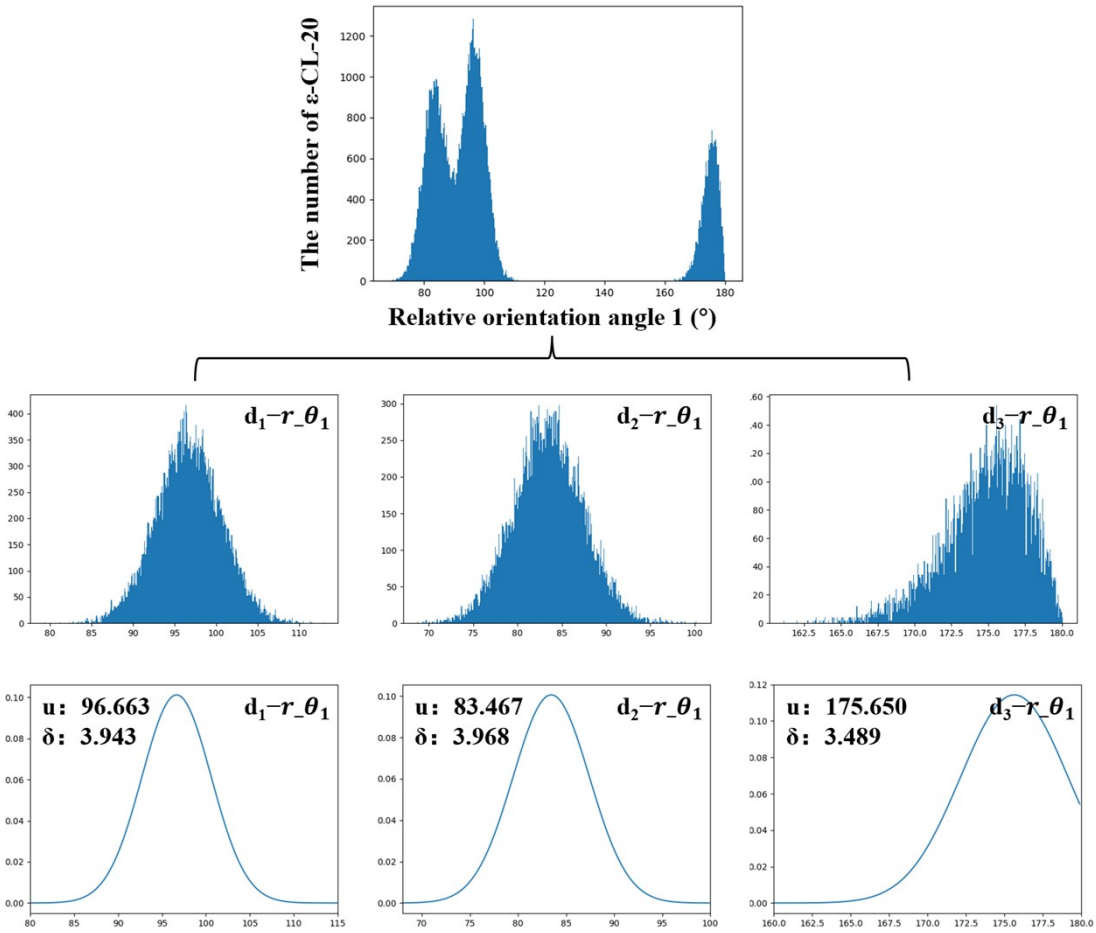

Figure S11. Schematic diagram of the Gaussian decomposition fitting for the relative orientational angle 1 distribution in ε-CL-20 molecular crystals.

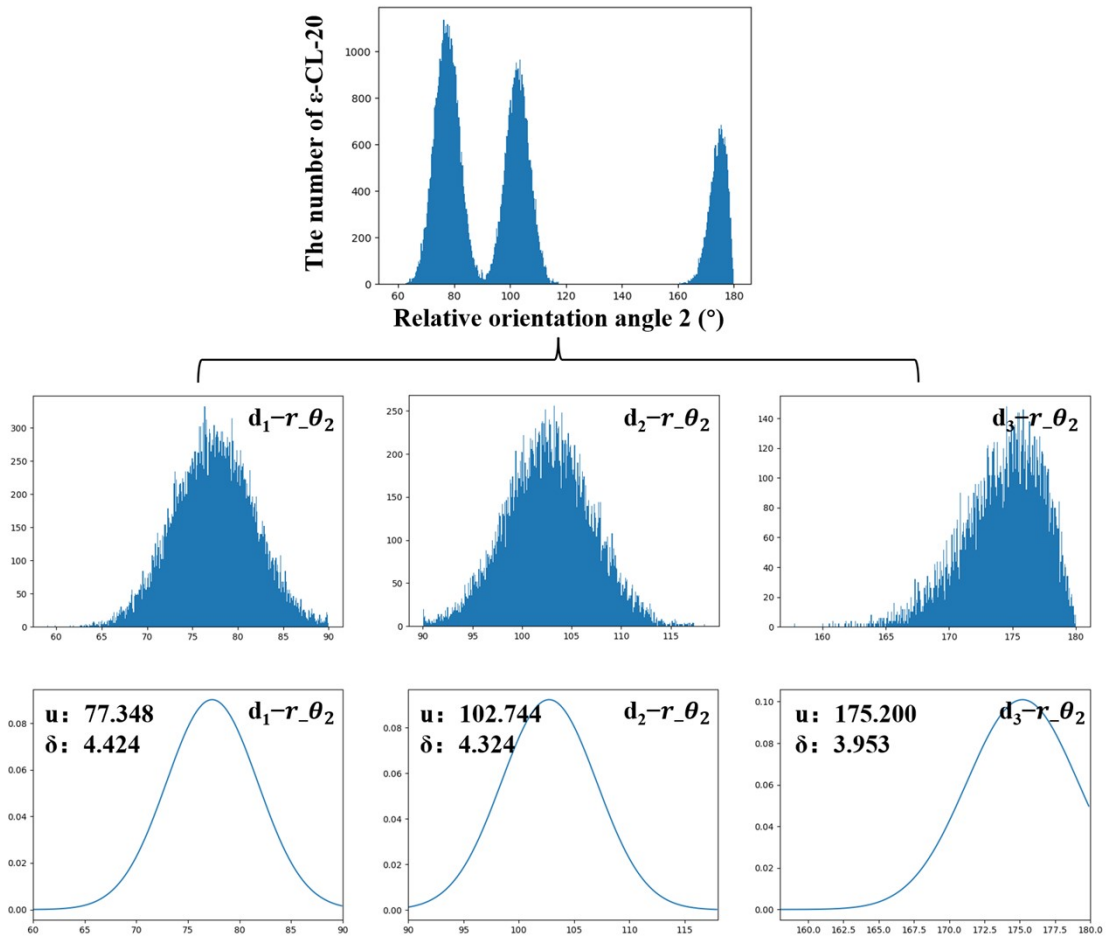

Figure S12. Schematic diagram of the Gaussian decomposition fitting for the relative orientational angle 2 distribution in ε-CL-20 molecular crystals.

Like the process for establishing the OPs of ε-CL-20, the expressions for β- and γ-CL-20 were derived. The decomposed distance distributions, relative bond angle distributions, and relative azimuthal angle distributions for β- and γ-CL-20, along with the means and standard deviations of the fitted Gaussian functions, are shown in Tables S4 and S5.

Table S4. Means and standard deviations of the Gaussian functions for the distance distribution, relative bond angle distribution, and relative azimuthal angle distribution in β-CL-20 molecular crystals.

Order Parameters	Expectation, Standard deviation (Å)	Order Parameters	Expectation, Standard deviation (Å)
d_1	u：6.927 σ：0.111	d_2	u：7.558 σ：0.136
$d_1\text{-}b\_\theta_1$	u1：37.213 σ1：2.859 u2：58.749 σ2：2.808 u3：120.628 σ3：2.846 u4：141.832 σ3：2.940	$d_2\text{-}b\_\theta_1$	u1：43.310 σ1：4.117 u2：103.523 σ2：4.099
$d_1\text{-}b\_\theta_2$	u1：26.097 σ1：3.041 u2：82.159 σ2：3.293 u3：98.772 σ3：3.277 u4：156.074 σ3：3.051	$d_2\text{-}b\_\theta_2$	u1：93.619 σ1：3.095 u2：128.620 σ2：3.427
$d_1\text{-}r\_\theta_1$	u：23.055	$d_2\text{-}r\_\theta_1$	u：175.780

	σ： 3.391		σ： 3.759
d_1-r_θ_2	u：95.544 σ： 4.602	d_2-r_θ_2	u：175.180 σ： 4.098

Table S5. Means and standard deviations of the Gaussian functions for the distance distribution, relative bond angle distribution, and relative azimuthal angle distribution in γ-CL-20 molecular crystals.

Order Parameters	Expectation, Standard deviation (Å)	Order Parameters	Expectation, Standard deviation (Å)
d_1	u：7.580 σ：0.134	d_2	u：6.677 σ：0.106
d_1-b_θ_1	u1：42.503 σ1：3.524 u2：83.260 σ2：3.285 u3：96.590 σ3：3.383 u4：137.514 σ3：3.504	d_2-b_θ_1	u1：61.567 σ1：3.420 u2：83.390 σ2：3.305 u3：96.865 σ3：3.412 u4：118.474 σ3：3.423
d_1-b_θ_2	u1：30.976 σ1：4.126 u2：84.375 σ2：3.975 u3：95.930 σ3：4.029 u4：149.053 σ3：4.032	d_2-b_θ_2	u1：62.552 δ1：3.222 u2：84.330 δ2：3.352 u3：95.780 δ3：3.403 u4：117.548 δ3：3.243
d_1-r_θ_1	u：109.490 δ： 4.171	d_2-r_θ_1	u：175.780 δ： 3.759
d_1-r_θ_2	u：53.771 δ： 5.805	d_2-r_θ_2	u：175.180 δ： 4.098

S4. Evolutions of polymorphic weight and free energy surface obtained from the WT-MetaD Simulations.

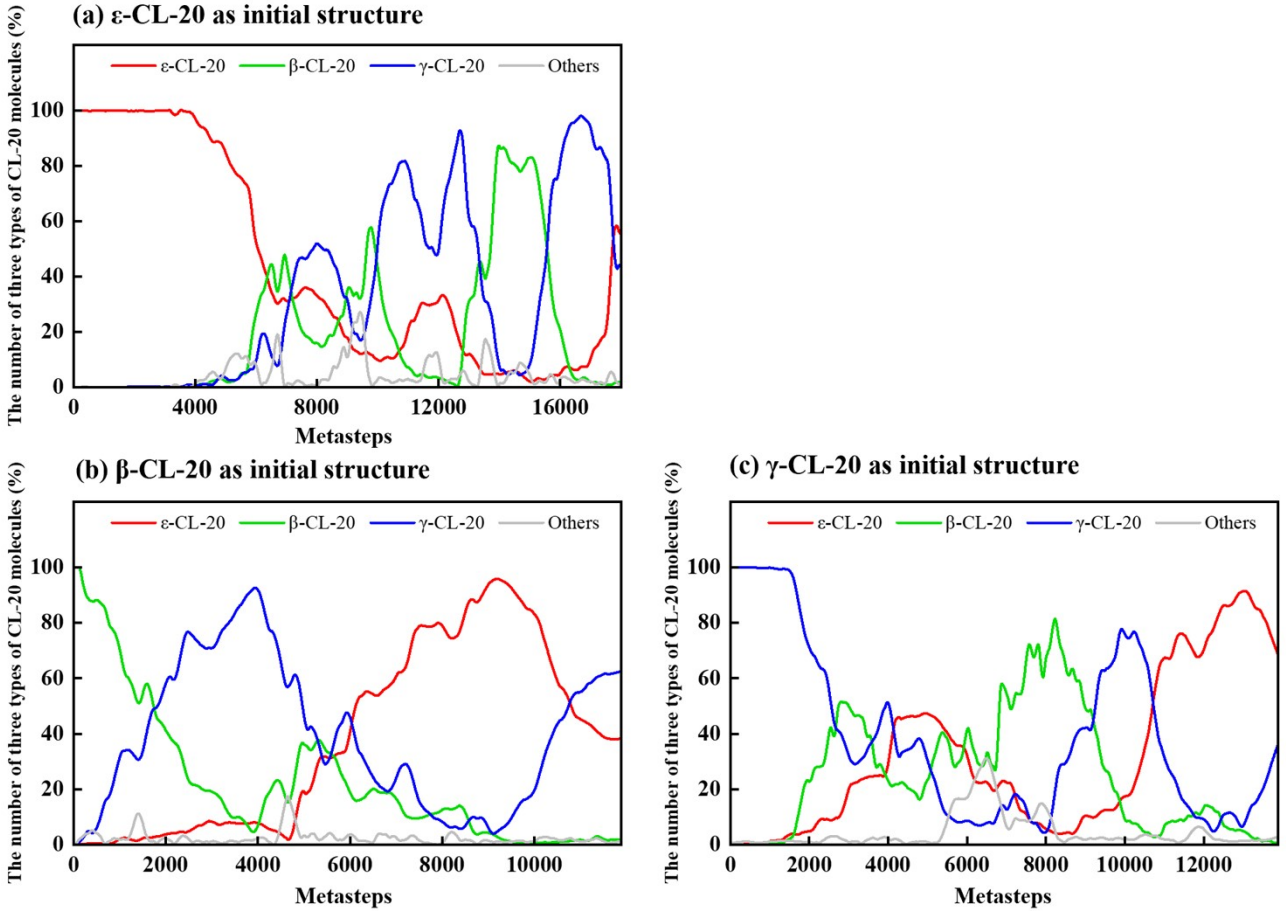

Figure S13. Molecular number variation during phase transitions of different polymorphs. The red curve represents the molecular number variation for ϵ-CL-20, the green curve represents the molecular number variation for β-CL-20, and the blue curve represents the molecular number variation for γ-CL-20. Transition simulations initiated from (a) ϵ-CL-20, (b) β-CL-20, and (c) γ-CL-20, respectively, which serve as references for verifying energy convergence.

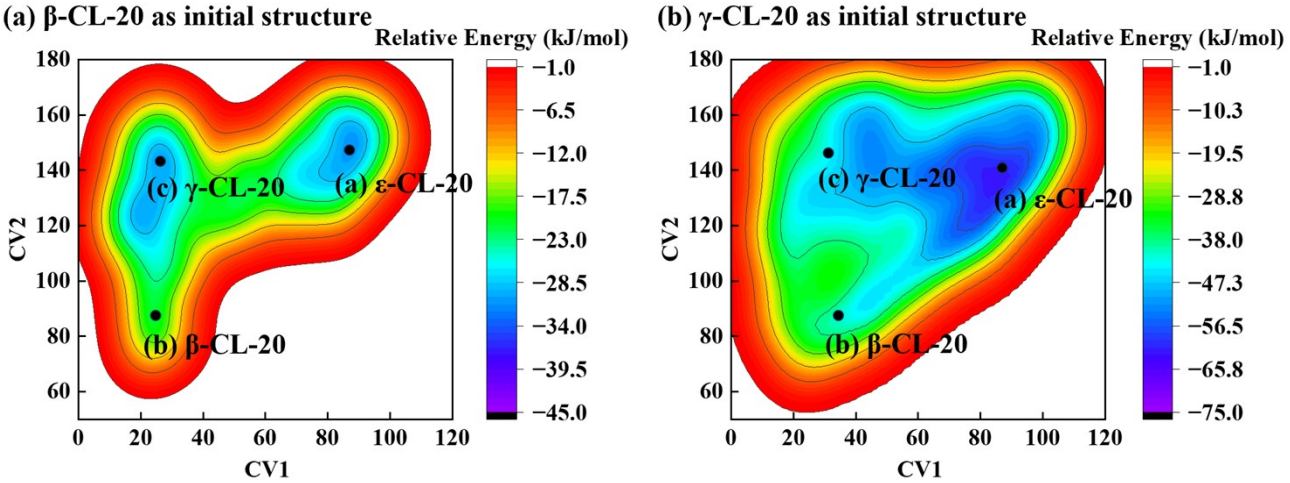

Figure S14. (a) 2D free energy surface with initial structure of β-CL-20. (b) 2D potential energy surface with initial structure of γ-CL-20. The positions of ε-, β-, and γ-CL-20 are both indicated on the two 2D potential energy surfaces.

S5. Root mean square deviation (RMSD) of centroid distance.

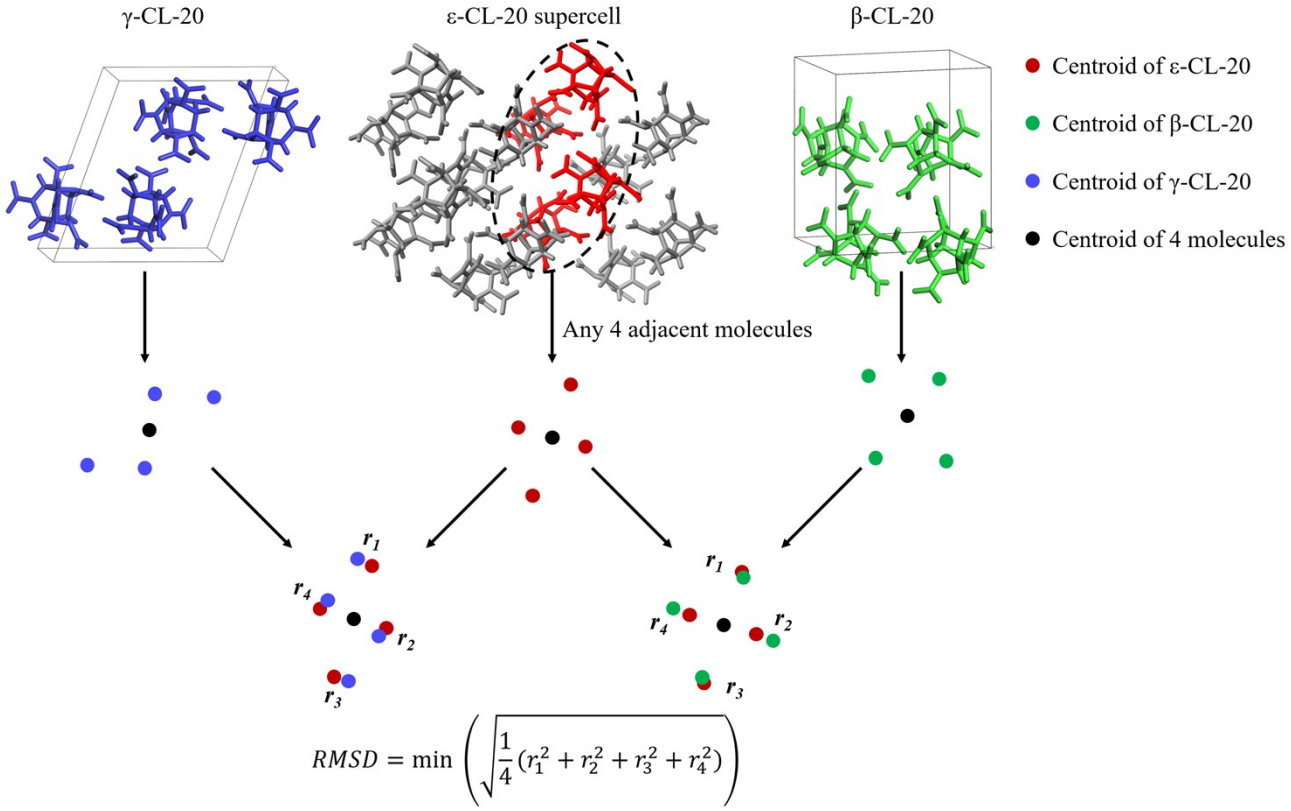

Figure S15. Schematic of RMSD calculations between four adjacent molecules in the ε-CL-20 supercell and those in β- and γ-CL-20 structures. The red, yellow, and blue points represent the molecular centroids of ε-, β-, and γ-CL-20, respectively. The black points represent the centroids of the systems containing four molecules.

The diagram outlines the root mean square deviation (RMSD) computation method to quantify structural differences. The calculations involve any four adjacent molecules selected from the ε-CL-20 supercell were compared to four molecules in β-CL-20 and γ-CL-20, respectively.

The RMSD was determined using the following formula:

$$RMSD = min\left(\sqrt{\frac{1}{4}(r_1^2 + r_2^2 + r_3^2 + r_4^2)}\right)$$

where r1, r2, r3, and r4 represent the distances between the centroids of corresponding molecules in ε-CL-20 and β- or γ-CL-20 when their overall centroids align. Upon fixing ε-CL-20, rotating the β- (or γ-) CL-20 around its overall centroid yields the minimal RMSD.